

Controlled self-aggregation of polymer-based nanoparticles employing shear flow and magnetic fields

David Toneian^{1,2}, Christos N. Likos², and Gerhard Kahl¹

¹Institute for Theoretical Physics, TU Wien, Wiedner Hauptstraße 8-10, A-1040 Vienna, Austria

²Faculty of Physics, University of Vienna, Boltzmanngasse 5, A-1090 Vienna, Austria

E-mail: david@toneian.com

Abstract. Star polymers with magnetically functionalized end groups are presented as a novel polymeric system whose morphology, self-aggregation, and orientation can easily be tuned by exposing these macromolecules simultaneously to an external magnetic field and to shear forces. Our investigations are based on a specialized simulation technique which faithfully takes into account the hydrodynamic interactions of the surrounding, Newtonian solvent. We find that the combination of magnetic field (including both strength and direction) and shear rate controls the mean number of magnetic clusters, which in turn is largely responsible for the static and dynamic behavior. While some properties are similar to comparable non-magnetic star polymers, others exhibit novel phenomena; examples of the latter include the breakup and reorganization of the clusters beyond a critical shear rate, and a strong dependence of the efficiency with which shear rate is translated into whole-body rotations on the direction of the magnetic field.

1. Introduction

Star polymers, a family of macromolecules where f polymeric arms (each consisting of n_A monomers) are tethered to a central, colloidal particle, have received a rapidly increasing share of interest within the soft matter community during the past years (see e.g. [1, 2]). The reason for their popularity rests both upon the tunability of their architecture via variations of f and/or n_A as well as upon the possibility to functionalize star polymers by selectively designing the polymeric arms [3]. This functionalization can, for instance, be realized by tethering block copolymers to the central colloid, leading to so-called telechelic star polymers [3]; alternatively, as recently put forward in [4], one can attach (super-para-)magnetic particles as terminal monomeric units onto each of the arms. This latter manner of functionalization is particularly attractive in that it allows for well-controlled and practically instantaneous tuning of the interaction, and hence of the system properties, via the external magnetic field, so that one does not have to rely on slow and inaccurate changes in temperature. In addition, it introduces strong anisotropy of the interactions between the endgroups, modifying thereby the morphology of the terminal aggregates from spherical into linear ones [4].

Star polymers show in their different architectures a broad range of interesting physical equilibrium properties; Examples include (i) the ability to cover in their single-molecule properties – by tuning their functionality f – the range of ultrasoft to spherical, essentially hard colloidal particles [1, 2], (ii) association, where telechelic star polymers form self-assembled, reconfigurable, soft patchy colloids, which then further self-organize at a supramolecular level into a variety of micellar or network-forming structures [3, 5], and (iii) the ability of the above-mentioned magnetically functionalized star polymers to form under equilibrium conditions clusters of particles (“valences”), whose number and size depend on f , n_A , and the strength and the orientation of the external magnetic field \mathbf{B} . The wealth of emerging scenarios (in terms of valence and molecular shape) has been thoroughly discussed in [4]. In addition to equilibrium situations, conventional star polymers exhibit a variety of intriguing properties in a stationary, non-equilibrium setup, as demonstrated in the investigations by Ripoll *et al.* [6], who have exposed these macromolecules

to shear forces by faithfully including hydrodynamic interactions: depending on the values of f and n_A , the particles show, upon increasing the shear rate $\dot{\gamma}$, strong deformations and distinctively different types of motion.

In this contribution, we extend these non-equilibrium simulations to the aforementioned magnetically functionalized star polymers and expose these particles both to shear forces as well as to an external magnetic field \mathbf{B} , considering three orientations of the latter relative to the shear flow direction ($\hat{\mathbf{e}}_x$), the shear gradient direction ($\hat{\mathbf{e}}_y$), and the vorticity direction ($\hat{\mathbf{e}}_z$). As compared to the related investigations on conventional star polymers [6], we face here an entirely new situation due to the emergence of patches which can or cannot be broken up under the influence of external fields, their stability being governed by an interplay between shear rate, magnetic field strength, and relative orientation of \mathbf{B} to the shear-cell geometry.

Employing the multi-particle collision dynamics (MPCD) technique [7], which incorporates hydrodynamic interactions, we provide evidence that conformational properties, such as the number, the size, and the location of the magnetic clusters, the shape of the macromolecule, or its flexibility can easily and accurately (but not necessarily independently from one another) be triggered via suitable combinations of the two above-mentioned external fields. With this contribution we thus introduce magnetically functionalized star polymers as a novel system of very flexible particles featuring specific numbers of self-associating aggregates with versatile and easily addressable conformational properties.

To the best of our knowledge, magnetically functionalized star polymers have not been synthesized in experiment, but realization of magnetic nanoparticles [8], their successful chemical coating and linkage [9], and a rich history of the study of other types of star polymers [10] make the synthesis of magnetically functionalized star polymers feasible and render them, as we hope to show in the following, interesting candidates for future experiments.

2. Model and Methods

In our investigations, we employ a bead-spring model for the magnetically functionalized star polymers: f linear polymer arms are attached to a core particle (index ‘C’), each of them containing n_A arm particles

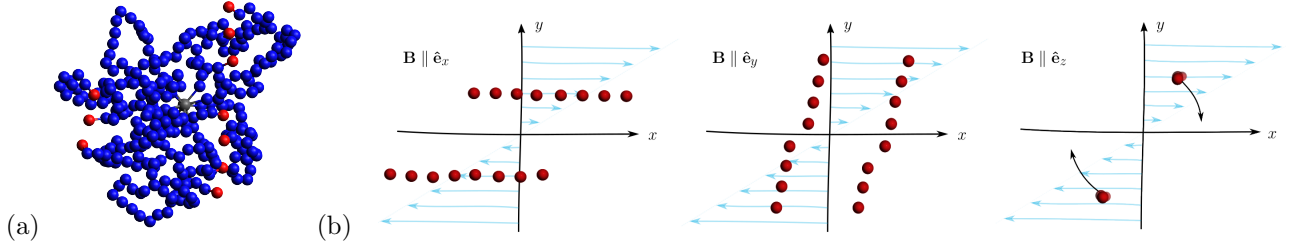


Figure 1. (color online) (a): Simulation snapshot, showing the star's core (gray), arm monomers (blue), and magnetic monomers (red). (b): Schematic representation of our simulation setup: a magnetically functionalized star polymer is exposed to shear flow (as specified in the text) and to an external magnetic field \mathbf{B} , pointing in independent experiments along the Cartesian axes. Blue: velocity profile of the flow, red: schematic representation of the super-paramagnetic end monomers, forming two magnetic clusters (suppressing the arm monomers and the central core bead, which would be situated approximately in the origin in this sketch). In the three panels, the magnetic field \mathbf{B} points along the flow, gradient, or vorticity direction (from left to right).

(index 'A'); to the end of each arm, a super-paramagnetic particle (index 'M') is attached. The steric interactions of all these spherical monomeric units have two concentric interaction ranges: an inner, impenetrable part with diameter D_α and an outer, soft part with range σ_α , with $\alpha = C, A,$ or M . The masses of all types of monomers are assumed to be equal in order to avoid introducing features dependent on specific mass asymmetries.

Any pair of monomers, separated by a distance r , interact via a modified Weeks-Chandler-Andersen (WCA) potential $V_{\text{WCA}}(r)$ [11], given by

$$V_{\text{WCA}}(r) = \begin{cases} V_0(r) & \text{if } r - D_{\alpha\beta} \leq 2^{1/6}\sigma_{\alpha\beta}, \\ 0 & \text{else} \end{cases},$$

$$V_0(r) = 4\epsilon_{\alpha\beta} \left[\left(\frac{\sigma_{\alpha\beta}}{r - D_{\alpha\beta}} \right)^{12} - \left(\frac{\sigma_{\alpha\beta}}{r - D_{\alpha\beta}} \right)^6 + \frac{1}{4} \right],$$

with $D_{\alpha\beta} = (D_\alpha + D_\beta)/2$, $\sigma_{\alpha\beta} = (\sigma_\alpha + \sigma_\beta)/2$, and $\epsilon_{\alpha\beta} = \sqrt{\epsilon_\alpha \epsilon_\beta}$, to be set to specific values in what follows.

Spring bonds between (i) the core monomer and the first arm monomer, (ii) adjacent arm monomers, and (iii) the last arm monomer and the functionalized monomer are modeled via the generalized finitely extensible non-linear elastic (FENE) potential [12, 13], specified via

$$V_{\text{FENE}}(r) = -\frac{1}{2}K_{\alpha\beta}R_{\alpha\beta}^2 \ln \left[1 - \left(\frac{r - l_{\alpha\beta}}{R_{\alpha\beta}} \right)^2 \right]; \quad (1)$$

here, $K_{\alpha\beta}$ specifies the interaction strength, $l_{\alpha\beta}$ is the equilibrium bond length between monomers α and β , and $R_{\alpha\beta}$ is the maximum deviation from $l_{\alpha\beta}$. In addition, the magnetic monomers interact via the standard dipole-dipole interaction, i.e.,

$$V_{\text{M}}(\mathbf{r}) = -\frac{\mu_0}{4\pi r^3} [3(\mathbf{m}_1 \cdot \hat{\mathbf{r}})(\mathbf{m}_2 \cdot \hat{\mathbf{r}}) - \mathbf{m}_1 \cdot \mathbf{m}_2]; \quad (2)$$

with \mathbf{m}_1 and \mathbf{m}_2 being the dipolar moments of two interacting particles which are separated by a vector \mathbf{r}

(with $r = |\mathbf{r}|$ and $\hat{\mathbf{r}} = \mathbf{r}/r$). The dipole moments are assumed to be equal in magnitude (i.e., $|\mathbf{m}_1| = |\mathbf{m}_2| = m$), and μ_0 is the vacuum permeability.

For reasons of simplicity, we assume that the moments of the super-paramagnetic particles are always perfectly aligned with the external, spatially homogeneous magnetic field, $\mathbf{B} = B\hat{\mathbf{e}}_{\mathbf{B}}$. With all this in mind, the expression (2) for $V_{\text{M}}(\mathbf{r})$ simplifies to

$$V_{\text{M}}(\mathbf{r}) = -\frac{\mu_0 m^2}{4\pi r^3} [3(\hat{\mathbf{e}}_{\mathbf{B}} \cdot \hat{\mathbf{r}})^2 - 1]. \quad (3)$$

We introduce the dimensionless magnetic parameter $\lambda = \mu_0 m^2 / (4\pi\sigma^3\epsilon)$, with the length and energy scales σ and ϵ defined below. λ represents the relative strength of the magnetic interaction compared with the other potentials, as well as the thermal and hydrodynamic interactions. Assuming, due to the super-paramagnetism, that $m \propto B$, one can consider $\lambda \propto B^2$ a measure of the magnetic field strength, and thus view dependencies on λ and $\hat{\mathbf{e}}_{\mathbf{B}}$ as dependencies on the external \mathbf{B} -field in (computer) experiments.

In an effort to reduce the large number of system parameters, we have used the following set of WCA-parameters which mimic a simple, yet reasonable model of a magnetically functionalized star polymer:

$$\epsilon_\alpha = k_{\text{B}}T = \epsilon \quad \text{with } \alpha = C, A, \text{ or } M,$$

$$D_C = 2a, \quad D_A = 0, \quad D_M = a, \quad \text{and}$$

$$\sigma_C = \sigma_A = \sigma_M = a = \sigma.$$

Here, T is the temperature, k_{B} is Boltzmann's constant, and a is the MPCD length unit, to be specified below \ddagger . For the FENE parameters we use $K_{\alpha\beta} = 30\epsilon_{\alpha\beta}\sigma_{\alpha\beta}^{-2}$ and

$$l_{\alpha\beta} = D_{\alpha\beta}, \quad R_{\alpha\beta} = 1.5\sigma_{\alpha\beta}, \quad \text{with } \alpha = C, A, \text{ or } M.$$

\ddagger $\sigma = a$ has been chosen in order to achieve, on average, a spatial separation of two monomers sufficient to place them in different MPCD collision cells.

To quantify the shape of the star polymer under arbitrary external conditions, we employ the radius of gyration tensor, \mathcal{S} , with elements $S_{\mu\nu}$ ($\mu, \nu = 1, 2, 3$)

$$S_{\mu\nu} = \frac{1}{N} \sum_{i=1}^N r_{\mu}^i r_{\nu}^i; \quad (4)$$

r_{μ}^i is the μ -th component of the Cartesian position vector of particle i with respect to the molecule's center of mass frame; $N = 1 + f(n_A + 1)$ is the total number of monomers. From the eigenvalues of this tensor, termed Λ_{α}^2 ($\alpha = 1, 2, 3$), and assuming, without loss of generality, that $\Lambda_1^2 \leq \Lambda_2^2 \leq \Lambda_3^2$, one can calculate the acylindricity c , the asphericity b , the radius of gyration R_g , and the relative shape anisotropy κ^2 of the macromolecule [14]:

$$c = \Lambda_2^2 - \Lambda_1^2 \quad b = \Lambda_3^2 - \frac{1}{2}(\Lambda_1^2 + \Lambda_2^2) \quad (5)$$

$$R_g = \sqrt{\Lambda_1^2 + \Lambda_2^2 + \Lambda_3^2} \quad \kappa^2 = \frac{1}{R_g^4} \left(b^2 + \frac{3}{4}c^2 \right).$$

Typical configurations of functionalized star polymers under *equilibrium* conditions, for different arm lengths (i.e., different values of n_A) and different values of λ under the influence of some external magnetic field are shown in figure 1 of [4]; a key observation is the emergence of columns of endgroup-monomers extending parallel to $\hat{\mathbf{e}}_{\mathbf{B}}$.

To shed light on the tunability of these particles under *non-equilibrium* conditions, we have exposed in this contribution a single functionalized star polymer to shear forces, assuming the flow direction, the velocity gradient direction, and the vorticity direction along the x -, y , and z -axes, respectively; the strength of the flow is measured by the shear rate $\dot{\gamma}$. In addition, we have applied an external magnetic field, \mathbf{B} , which we have assumed in distinct computer experiments to be oriented along each of the Cartesian axes; see figure 1 for a schematic representation.

To avoid a scan of the high-dimensional parameter space, we have restricted ourselves to the case of star polymers with a functionality $f = 10$, each arm being formed by $n_A = 30$ monomers – a situation which is computationally very tractable and still exhibits rich physics and phenomenology already in the equilibrium case [4]. For the reduced magnetic interaction strength λ two values have been assumed, namely $\lambda = 100$ and $\lambda = 200$. From the diagrams of states (as they are shown in [4]) we know that for this set of parameters, star polymers form under equilibrium conditions two to three magnetic column-shaped clusters; these are assemblies of interacting magnetic end-monomers, aligned along the external magnetic field, where two magnetic beads are considered to be part of the same cluster if their interparticle distance is at most $2.5a$.

In the Multi-Particle Collision Dynamics (MPCD) technique, the macromolecule is surrounded by microscopic fluid particles of mass m_f which are considered point particles; their positions and momenta are not constrained to a lattice (for details cf. [7]). In this simulation technique, two steps are carried out alternately: (i) in the *streaming step*, the point particles move ballistically for a time Δt , such that $\mathbf{r}_i(t + \Delta t) = \mathbf{r}_i(t) + \mathbf{v}_i(t)\Delta t$, $\mathbf{r}_i(t)$ and $\mathbf{v}_i(t)$ being the position and velocity of particle i , respectively. (ii) In the *collision step*, interaction takes place: in the variant of MPCD that we have employed in this contribution, Stochastic Rotation Dynamics, the point particles are sorted, according to their instantaneous positions $\mathbf{r}_i(t)$, into *collision cells*, i.e. cubic boxes of side length a , which tessellate the simulation volume. Then, for each collision cell k , one transforms the velocities of all particles i in that cell according to the rule $\mathbf{v}_i(t) \mapsto \mathbf{V}_k(t) + \mathcal{R}(k, t, \alpha) [\mathbf{v}_i(t) - \mathbf{V}_k(t)]$, where $\mathbf{V}_k(t) = (\sum_{i \in \text{cell}_k} m_i \mathbf{v}_i(t) / \sum_{i \in \text{cell}_k} m_i)$ is the center-of-mass velocity of collision cell k , m_i is the mass of particle i , and $\mathcal{R}(k, t, \alpha)$ is a rotation matrix about a randomly chosen axis and fixed angle α , with independent choices for each collision cell k and time t . In order to suspend the star polymer in this MPCD fluid, its beads are treated like fluid particles, except that their masses are $m_b = 5m_f$, and – instead of ballistic streaming – the intra-star forces are integrated in five consecutive iterations of a velocity-Verlet algorithm [15], each with timestep $\Delta t/5$.

Simulations were initialized with equilibrium configurations of the stars and a random fluid configuration; representative data was taken only after an equilibration period to avoid correlations with the initial state. The simulation volume was chosen to be cubic and of side length $30a$. Lees-Edwards boundary conditions [16] were employed to enforce a shear flow. Units are chosen such that $a = 1$, $m_f = 1$, and $k_B T = 1$, the temperature T being enforced via the Maxwell-Boltzmann scaling thermostat [17]. The pure fluid's mass density was set to $\varrho = 10$, such that in total $10 \times 30^3 = 270 \times 10^3$ MPCD fluid particles were simulated. The rotation angle α was set to 2.27 radians, corresponding to approximately 130 degrees. The *OpenMPCD* simulation package used can be found at [18].

3. Results

We find that the observed conformational and dynamic properties can qualitatively be classified into four categories: (i) the mean number of magnetic clusters, N_C , which is of particular importance and thus warrants separate treatment, (ii) quantities that are largely controlled by N_C , (iii) quantities that are

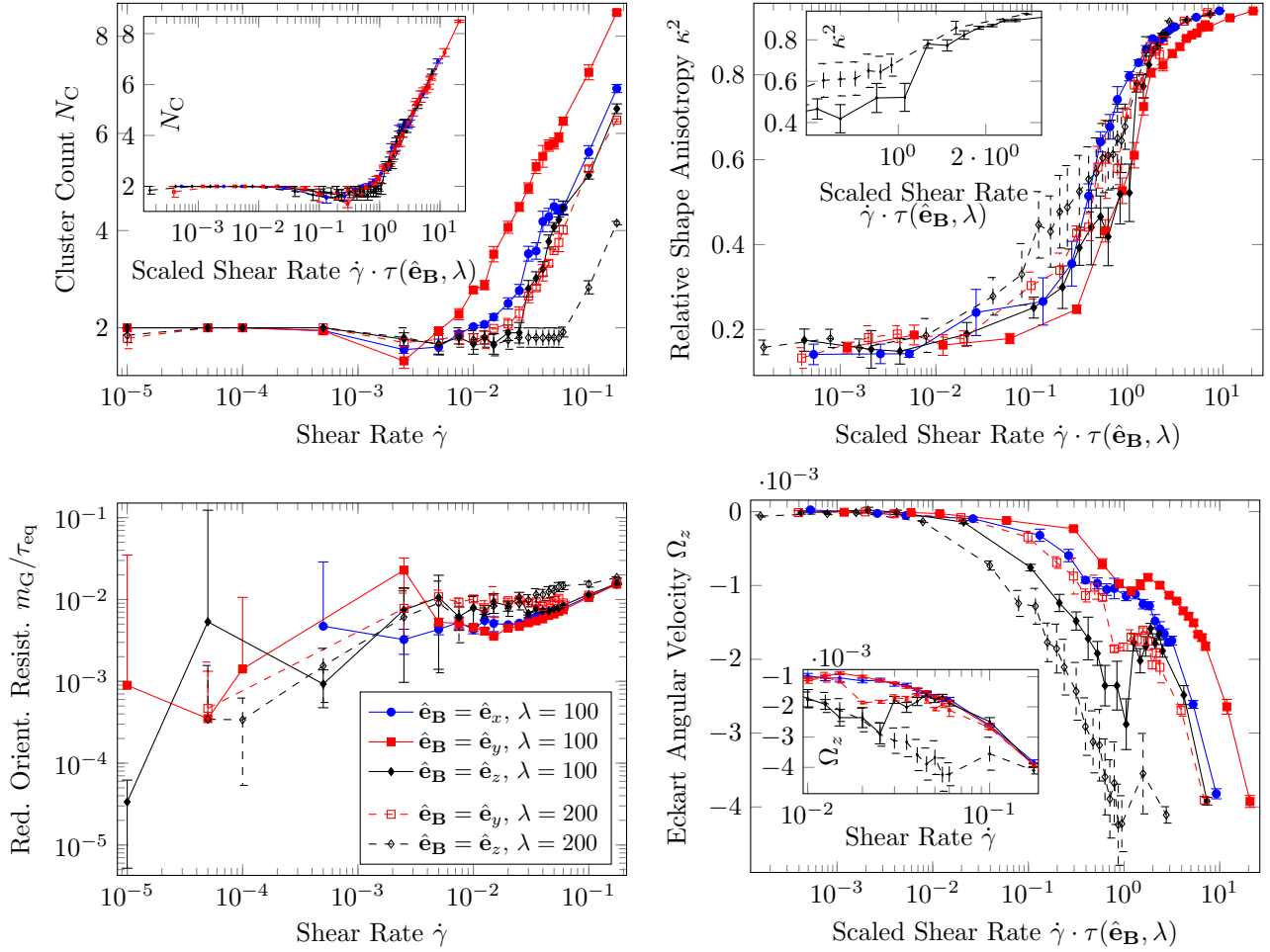


Figure 2. (color online) Specific quantities that characterize the magnetically functionalized star polymer as functions of the shear rate $\dot{\gamma}$ for different orientations of the external field $\hat{\mathbf{e}}_{\mathbf{B}}$ and values of its relative strength, λ (as labeled): top-left – number of magnetic clusters N_C , top-right – relative shape anisotropy κ^2 , inset showing a zoomed-in view for $\hat{\mathbf{e}}_{\mathbf{B}} = \hat{\mathbf{e}}_z$; bottom-left – reduced orientational resistance m_G/τ_{eq} , and bottom-right – Eckart angular velocity around z -axis Ω_z , inset showing data with unscaled shear rates $\dot{\gamma}$ in a zoomed-in region. Scaled shear rates are constructed via an empirically determined $\tau(\hat{\mathbf{e}}_{\mathbf{B}}, \lambda)$ such that the N_C curves collapse to a master curve (cf. inset in top-left figure). The legend in the bottom-left panel applies equally to all panels and insets. See main text for details.

unaffected by the presence of magnetic moments in the model, and (iv) quantities that, *on top* of an N_C -dependence, are sensitive to the orientation of the external magnetic field $\hat{\mathbf{e}}_{\mathbf{B}}$ relative to the shear flow and shear gradient direction.

3.1. Mean Number of Clusters N_C

The main plot in the top-left panel of figure 2 shows the mean number of clusters, N_C , as a function of the shear rate $\dot{\gamma}$. For low $\dot{\gamma}$ -values, the mean cluster count is roughly 2, up until a critical shear rate $\dot{\gamma}^*$ is reached, which depends on the orientation $\hat{\mathbf{e}}_{\mathbf{B}}$ and strength (encoded in λ) of the external magnetic field. At this $\dot{\gamma}^*$, shear-induced forces overcome the attractive magnetic interactions, breaking up columns of end-monomers (which form along the $\hat{\mathbf{e}}_{\mathbf{B}}$ direction) into

successively smaller, more stable units as the shear rate is increased; to be more specific, we observe $N_C \propto \ln(\dot{\gamma})$. This critical $\dot{\gamma}^*$ is largest for $\hat{\mathbf{e}}_{\mathbf{B}} = \hat{\mathbf{e}}_z$ and smallest for $\hat{\mathbf{e}}_{\mathbf{B}} = \hat{\mathbf{e}}_y$, where the magnetic columns are particularly exposed to the shear flow gradient (cf. figure 1). Furthermore, $\dot{\gamma}^*$, or equivalently, the robustness of magnetic clusters, increases with λ . The inset shows that, upon scaling the shear rate with an empirical $\hat{\mathbf{e}}_{\mathbf{B}}$ - and λ -dependent factor $\tau(\hat{\mathbf{e}}_{\mathbf{B}}, \lambda)$, all curves collapse onto a master curve, with the scaling chosen such that $\dot{\gamma}^*(\hat{\mathbf{e}}_{\mathbf{B}}, \lambda) \cdot \tau(\hat{\mathbf{e}}_{\mathbf{B}}, \lambda) \approx 1$.

3.2. N_C -Controlled Quantities: Shape Descriptors

The shape descriptors [cf. equation (5)], when viewed as functions of the scaled shear rate, exhibit comparable qualitative behavior for various orientations $\hat{\mathbf{e}}_{\mathbf{B}}$ and

magnetic interaction strengths λ . This is significant in that the shape is largely determined by the number of magnetic columns formed in a given situation, but is otherwise relatively unaffected by the details of the magnetic interaction.

The top-right panel of figure 2 shows the relative shape anisotropy κ^2 as a representative member of this category of quantities. A value of κ^2 near 0 would roughly be indicative of a spherically symmetric arrangement of the star polymer's beads; even for low shear rates $\dot{\gamma}$, this condition is not met, since the magnetic columns formed by the end-monomers break rotational symmetry, as they align with the external magnetic field. For higher shear rates, the polymer is strongly elongated along the flow direction. Also, note that there is a sudden increase in κ^2 at $\dot{\gamma}(\hat{\mathbf{e}}_{\mathbf{B}}, \lambda) \cdot \tau(\hat{\mathbf{e}}_{\mathbf{B}}, \lambda) \approx 1$, i.e. at the critical shear rate $\dot{\gamma}^*$ where magnetic clusters start breaking apart, particularly pronounced for $\hat{\mathbf{e}}_{\mathbf{B}} = \hat{\mathbf{e}}_z$ (see panel inset). Conversely, given the rather well-defined dependence of N_C on \mathbf{B} and $\dot{\gamma}$, one can manipulate the shape and size of the star polymers by tuning the external fields in their strength and/or relative orientation.

3.3. Universal Properties: Orientational Resistance

One can measure the extent of alignment between the flow direction ($\hat{\mathbf{e}}_x$) and the major axis of the instantaneous configuration of the star polymer, i.e. the eigenvector associated with the largest eigenvalue Λ_3^2 of \mathcal{S} , and denote the corresponding angle χ ; then, one can define the orientational resistance $m_G = \dot{\gamma}\tau_{\text{eq}} \tan(2\chi)$, where τ_{eq} is the longest relaxation time of the star polymer in equilibrium.

The bottom-left panel of figure 2 shows m_G/τ_{eq} as a function of $\dot{\gamma}$. For sufficiently large shear rates ($\dot{\gamma} \gtrsim 10^{-2}$ in inverse MPCD time units), the orientational resistance follows a power-law $m_G \propto \dot{\gamma}^\mu$ with a characteristic exponent $0.4 < \mu < 0.6$. This behavior is shared by the majority of polymeric systems (each with a corresponding value of μ), ranging from linear chains to block copolymers, randomly cross-linked single-chain nanoparticles, dendrimers, and non-magnetic star polymers [6, 19, 20, 21, 22]. Thus, while the exponent μ varies with \mathbf{B} , the characteristic power-law of star polymers is conserved despite the addition of a magnetic interaction and the associated introduction of another distinguished axis.

While parts of the literature predict [23] or report [6] m_G approaching a constant plateau for low $\dot{\gamma}$, the high fluctuations observed in our data for low shear rates allow neither confirmation nor dismissal of this claim.

3.4. $\hat{\mathbf{e}}_{\mathbf{B}}$ -Sensitivity Beyond N_C : Angular Velocity

Although the star's shape is largely determined by N_C , as discussed above, the rotational dynamics of the star are peculiar in that they have an additional dependence on the orientation of $\hat{\mathbf{e}}_{\mathbf{B}}$: When considering the angular velocities ω_α around the Cartesian axes α , or more appropriately, the Eckart-frame angular velocities Ω_α – constructed so as to remove spurious contributions by vibrational modes to the (apparent) angular velocity [24, 25, 26] – one finds that there is no net rotation around the x (shear flow direction) and y (shear gradient direction) axes, but a significant rotation $\Omega_z \neq 0$ (shear vorticity direction); this fact additionally and decisively distinguishes the case $\hat{\mathbf{e}}_{\mathbf{B}} = \hat{\mathbf{e}}_z$ from the other ones, even when scaling the shear rates (cf. figure 1 and bottom-right panel in figure 2).

In particular for $\hat{\mathbf{e}}_{\mathbf{B}} = \hat{\mathbf{e}}_z$, the magnetic interaction parameter λ plays no role below the critical shear rate $\dot{\gamma}^*$ (see inset), and as soon as magnetic columns start breaking up, the different curves approach a common master curve, corresponding to the case of little to no magnetic clustering. The most pronounced change in (Eckart) angular velocity occurs, again, at $\dot{\gamma} = \dot{\gamma}^*$ (cf. inset) or $\dot{\gamma}(\hat{\mathbf{e}}_{\mathbf{B}}, \lambda) \cdot \tau(\hat{\mathbf{e}}_{\mathbf{B}}, \lambda) \approx 1$ (cf. main panel), respectively.

4. Conclusions and Outlook

Decorating the arms of star polymers with magnetic particles opens up a rich, new facet of the phenomenology of polymer physics. The resulting magnetically functionalized star polymers are sensitive to both direction and intensity of an external magnetic field, as well as to the relative orientation and strength of shear flow. Said sensitivity manifests in the self-aggregation behavior of columns of the star's magnetic monomers, and the stability of the resulting magnetic columns. This in turn largely determines size, shape, anisotropy, and dynamic responses, some aspects of which (e.g. orientational resistance) behave qualitatively as in the non-magnetic case, while others (e.g. whole-body rotation) exhibit entirely novel phenomenology.

The tunability of the star conformation, anisotropy, and of the stability of magnetic aggregates via manipulation of the external magnetic field \mathbf{B} allows for new avenues in which (computer) experiments can be conducted. For example, upcoming research will discuss self-aggregation of magnetic columns in dense solutions of magnetic stars, how changes in the external fields can influence e.g. rheology or the formation of large-scale structures in a given system, and what types of phase behavior can be observed. Possible applications might include micro-fluidic devices, such as micro-mixers with tunable efficiency due solely to the geometry of flow and magnetic field.

Acknowledgments

The authors acknowledge financial support by the Austrian Science Fund FWF within the SFB ViCoM (F41) and computing time by the Vienna Scientific Cluster. The authors thank Ronald Blaak (Clermont-Ferrand) for helpful discussions and Angela Koffler for her help in creating figure 1. D.T. and G.K. acknowledge financial support by the FWF under Proj. No. I3846-N36.

References

- [1] Likos C N 2006 *Soft Matter* **2** 478
- [2] Vlassopoulos D and Cloitre M 2014 *Curr. Opin. Colloid Interface Sci.* **19** 561
- [3] Gárlea I C, Bianchi E, Capone B, Rovigatti L and Likos C N 2017 *Curr. Opin. Colloid Interface Sci.* **30** 1
- [4] Blaak R and Likos C N 2018 *Eur. Phys. J. E* **41** 3
- [5] Bianchi E, Capone B, Kahl G and Likos C N 2015 *Faraday Discuss.* **181** 123
- [6] Ripoll M, Winkler R G and Gompper G 2006 *Phys. Rev. Lett.* **96** 188302
- [7] Gompper G, Ihle T, Kroll D M and Winkler R G 2009 *Adv. Polym. Sci.* **211** 1
- [8] Wang H, Yu Y, Sun Y and Chen Q 2011 *Nano* **6** 1
- [9] Zhou Z, Liu G and Dehui H 2009 *ACS Nano* **3** 165
- [10] Hadjichristidis N, Pitsikalis M, Iatrou H, Driva P, Sakellariou G and Chatzichristidi M 2012 *Polymer Science: A Comprehensive Reference* **6** 29
- [11] Weeks J D, Chandler D and Andersen H C 1971 *J. Chem. Phys.* **54** 5237
- [12] Bird R B, Curtiss C F, Armstrong R C and Hassager O 1987 *Dynamics of Polymeric Liquids* vol 2 *Kinetic Theory* (New York: John Wiley & Sons)
- [13] Warner H R Jr 1972 *Ind. Eng. Chem. Fundam.* **11** 379
- [14] Theodorou D N and Suter U W 1985 *Macromolecules* **18** 1206
- [15] Frenkel D and Smit B 2002 *Understanding Molecular Simulation* (San Diego: Academic Press)
- [16] Lees A W and Edwards S F 1972 *J. Phys. C: Solid State Phys.* **5** 1921
- [17] Huang C C, Chatterji A, Sutmann G, Gompper G and Winkler R G 2010 *J. Comput. Phys.* **229** 168
- [18] <https://openmpcd.org>
- [19] Formanek M and Moreno A J 2018 *Single-Chain Nanoparticles under Homogeneous Shear Flow* arXiv:1812.03233 [cond-mat.soft]
- [20] Huang C-C, Winkler R G, Sutmann G and Gompper G 2010 *Macromolecules* **43** 10107
- [21] Nikoubashman A and Likos C N 2010 *Macromolecules* **43** 1610
- [22] Jaramillo-Cano D, Formanek M, Likos C N and Camargo M 2018 *J. Phys. Chem. B* **122** 4149
- [23] Aust C, Kröger M and Hess S 1999 *Macromolecules* **32** 5660
- [24] Eckart C 1935 *Phys. Rev.* **47** 552
- [25] Louck J D and Galbraith H W 1976 *Rev. Mod. Phys.* **48** 69
- [26] Sablić J, Delgado-Buscalioni R and Praprotnik M 2017 *Soft Matter* **13** 6988